Environ Health Perspect

DOI: 10.1289/EHP11068

Supplemental Material

Predicting the Effects of Climate Change on Dengue Vectors Densities in Southeast Asia through Process-Based Modeling

Lucas Bonnin, Annelise Tran, Vincent Herbreteau, Sébastien Marcombe, Sébastien Boyer, Morgan Mangeas, and Christophe Menkes

Table of Contents

Figure S4. Entomological survey sampling. Sampling locations in Phnom (Cambodia) Penh and Vientiane (Lao PDR) are displayed with red dots.

Figure S5. Contemporary climate seasonal variations at sampling sites in Phnom Penh (Cambodia) and Vientiane (Lao PDR).

Figure S6. Contemporary temperature and precipitations in Southeast Asia. Spatial and seasonal variations of temperature and precipitation from contemporary data.

Figure S7. Projected temperature and precipitations in Southeast Asia. Spatial and seasonal variations of climate projections at the end of the century following SSP1 2.3 and SSP3 7.0 (averages of the nine climate models). Diagonal hashing represent grid cells where anomalies associated with the nine climate models are significantly different from 0 (Student's t-test, p-value < 0.05).

Figure S8. Modeled *Ae. albopictus* and *Ae. aegypti* adult female densities in Southeast Asia, based on contemporary climate. Spatial and seasonal variations of modeled *Aedes adult* female density (top: *Ae. albopictus*; bottom: *Ae. aegypti*), based on contemporary climate data input.

Figure S9. Modeled *Ae. albopictus* and *Ae. aegypti* adult female densities in Southeast Asia, based on future projections. Panels describe projections of modeled *Aedes* adult female density at the end of the century (2081-2100) according to SSP1 2.6 and SSP3 7.0. Percentage changes correspond to ratios of projected modeled density over contemporary modeled densities, averaged over the nine simulations associated with the nine climate models. Positive (red) and negative (blue) percentage changes correspond respectively to higher and lower predicted mosquito density compared to the contemporary situation. Purple grid cells correspond to percentage changes greater than a threshold of 130%, mostly corresponding to areas of null to very low contemporary adult female density. Diagonal hashing represent grid cells where percentage changes associated with the nine climate models are significantly different from 0 (Student's t-test, p-value < 0.05).

Figure S10. Contemporary climate and future projections during summer and winter months. Panels A describe the spatial variations of contemporary temperature and precipitation in summer (April, May, June) and winter months (December, January, February). Panels B describe projections of temperature and precipitation averaged over the nine climate models in summer and winter months at the middle (2041-2060) and end of the century (2081-2100) according to SSP1 2.6 and SSP3 7.0. Diagonal hashing represent grid cells where anomalies associated with the nine climate models are significantly different from 0 (Student's t-test, p-value < 0.05).

Figure S11. Evolution of modeled Aedes density anomalies. Densities of *Ae. albopictus* and *Ae. aegypti* were modeled from climate data averages from all climate models, along the SSP3 7.0 pathway and for four periods to the end of the century. Percentage changes were calculated as a ratio of projected densities over contemporary densities, averaged over the nine simulations associated with the nine climate models. Diagonal hashing represent grid cells where percentage changes associated with the nine climate models are significantly different from 0 (Student's t-test, p-value < 0.05).

Figure S12. Comparison of modeled Aedes density anomalies across Shared Socio Economic Pathways. Densities of *Ae. albopictus* and *Ae. aegypti* were modeled over climate data averages from all climate models, for SSP1 2.6, SSP2 4.5, SSP3 7.0 and SSP5 8.5 and for the 2081-2100 period. Percentage changes were calculated as a ratio of projected densities over contemporary densities, averaged over the nine simulations associated with the nine climate models. Diagonal hashing represent grid cells where percentage changes associated with the nine climate models are significantly different from 0 (Student's t-test, p-value < 0.05).

Figure S13. Spatial trends of the future evolution of Aedes albopictus density versus topography. Percentage changes correspond to ratios of projected modeled *Ae. albopictus* density in summer months (2081-2100 SSP3 7.0) over contemporary modeled densities, averaged over the nine simulations associated with the nine climate models. Positive (red) and negative (blue) percentage changes correspond respectively to higher and lower predicted mosquito density compared to the contemporary situation. Contour lines represent the 300 m and 600 m isopleths.

Figure S14. Evolution of projected climate across the 21st century following four Shared Socio-Economic Pathways scenarios. Grid cells were split in two groups considering their elevation (Highlands: elevation < 600 m, Lowlands: elevation > 600 m). For each variable (temperature and precipitation), scenario, period and month, points and bars represent respectively mean and standard deviation of percentage change values associated to all climate models and all grid cells.

Figure S15. Effects of climate mitigation measures on *Aedes* densities. Process-based model simulations were performed over various constant values of temperature and precipitations. Model outputs were extracted after 30 days of simulation and plotted against corresponding temperature and precipitations (Panels A and C). Changes in temperature and precipitation associated with a transition from SSP3 7.0 to SSP1 2.6 at specific locations and season at the end of the century (2081-2100) are represented with white dots and arrows. Changes in *Ae. aegypti* and *Ae. albopictus* adult densities corresponding to a transition from SSP3 7.0 to SSP1 2.6 at the end of the century are mapped respectively in panels B and D.

Figure S16. Lengthening/shortening of the *Aedes* high density season. For both species, the median value of daily contemporary density was extracted for each grid cell, thus corresponding to the value at which contemporary densities are greater for 183 days of the year (6 months). For each grid cell, considering a 6-month long season of high contemporary adult density, the length of the season at the 2081-2100 horizon was considered as the number of days projected densities (SSP3 7.0) were greater than the contemporary median value. The lengthening/shortening of the season was assessed as the number of days longer/shorter than the 183 days of the contemporary season. Here are displayed in red and blue the areas where the model respectively predicts a lengthening and a shortening of *Ae. aegypti's* and *Ae. albopictus's* season. The values of season lengthening and shortening for each grid cell are displayed for both species as a boxplot (right panel). Boxes extend from quartiles Q1 to Q3, whiskers extend to 1.5 x (Q3 - Q1) from edges of the box. Overall median values are displayed as green bars and correspond to an overall lengthening of 10 days for *Ae. aegypti* and an overall shortening of 4 days for *Ae. albopictus*.

Figure S17. Process-based model's underlying transition and mortality functions as a function of temperature. Panels describe mortality and transition rates between life stages as a function of temperature, as used by the process-based model to simulate population dynamics of *Ae. albopictus* and *Ae. aegypti*.

Figure S18. Comparison of temperature-dependent transition rates used in process-based models. Temperature-dependent transition rates used in the model developed by Liu-Helmersson et al. (2019), were compared to those used in the present study. Although the two models differed in several aspects, notably on the number of life stages considered, comparing the functions describing transitions rates is still pertinent.

Table S1. Species Distribution Models quality metrics.

References

Figure S1. Study area. The study area covered Southeast Asia and was restricted to the countries of Myanmar, Lao PDR, Thailand, Cambodia and Vietnam. Borders are displayed here in red dotted lines and the color scale represents elevation. Black lines represent the 600 m contour line.

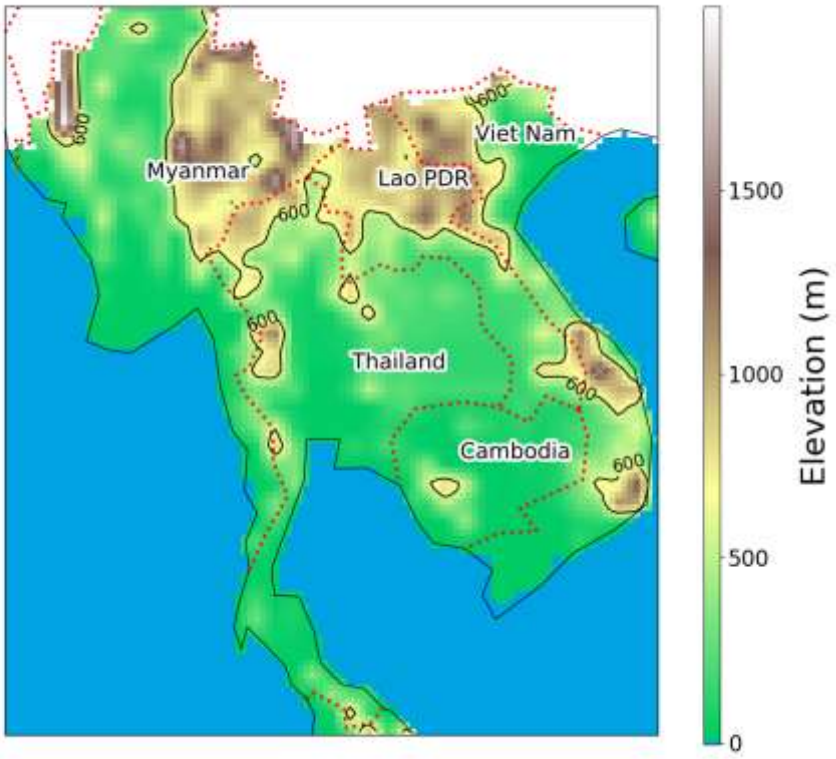

Figure S2. Process-based model diagram. Adapted from Figure 2 from Tran et al. (2020).[1] In blue, the aquatic stages (*E*: eggs, *L*: larvae, *P*: pupae); in orange, the adult female stages (A_{em}: emerging, A_1: nulliparous, A_2: parous, with *h*: host-seeking, *g*: resting, *o*: ovipositing).

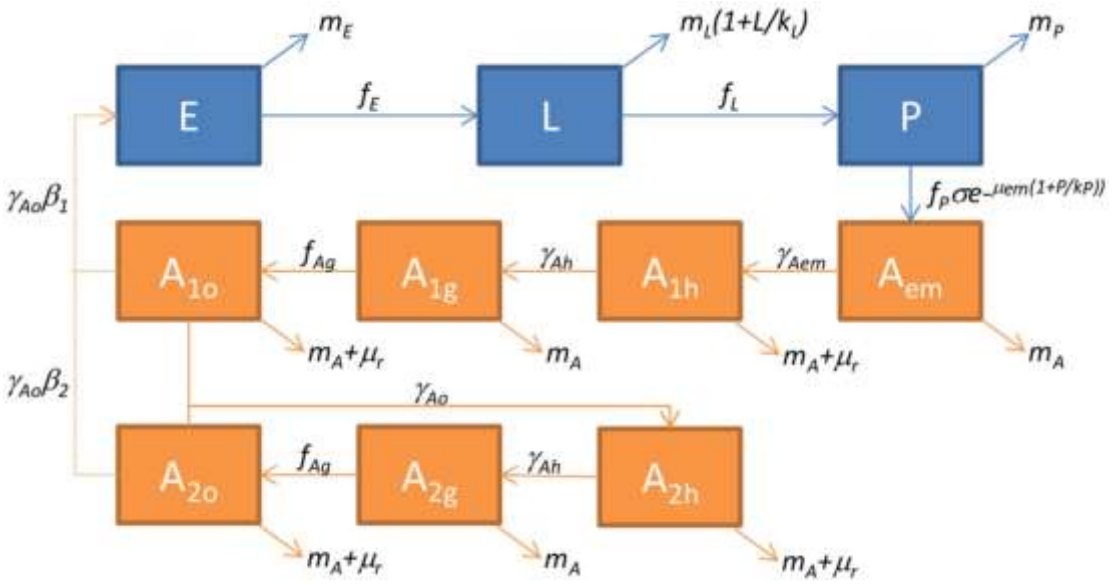

Figure S3a. Species Distribution Models predictions. An Ensemble Modeling approach was used to produce spatial predictions of the probability of observation of both species. For each species, the mean of predictions from the 30 models weighted by their AUC score (provided the model's AUC was greater than a threshold = 0,85) were computed to produce the final output. Maps of predicted probability of observation were thus computed for *Ae. aegypti* and *Ae. albopictus*. The dataset used to build the models are displayed as green and grey circles, respectively corresponding to true occurrences and to randomly-generated pseudo-absences.

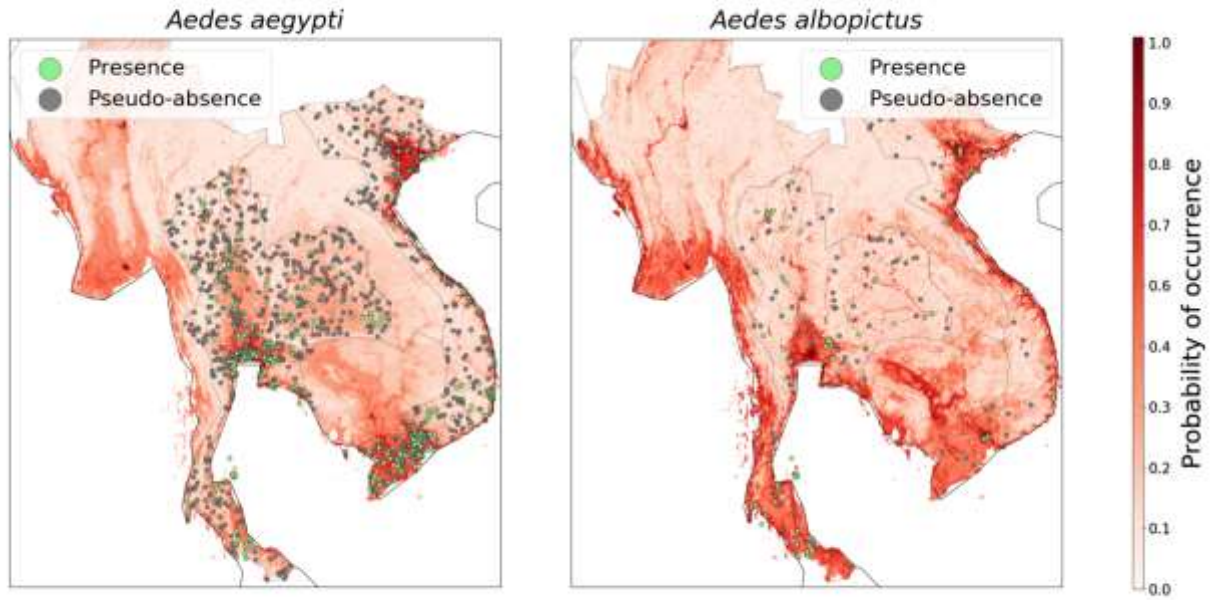

Figure S3b. Species Distribution Models partial dependency to proportion of Impervious Surface. Ensemble model predictions were computed for a range of values for the feature of interest (proportion of Impervious Surface), while setting other features values to observations. This resulted in a set of *N* response curves (faded lines, red for *Ae. aegypti*, blue for *Ae. albopictus*), *N* being the number of observations in the dataset (corresponding to occurrences and pseudo-absences). Solid lines represent the average response. Rugs are displayed respectively at the top and bottom of the plot to show the distribution of values of the feature of interest in the *Ae. aegypti* and *Ae. albopictus* datasets, in green for values

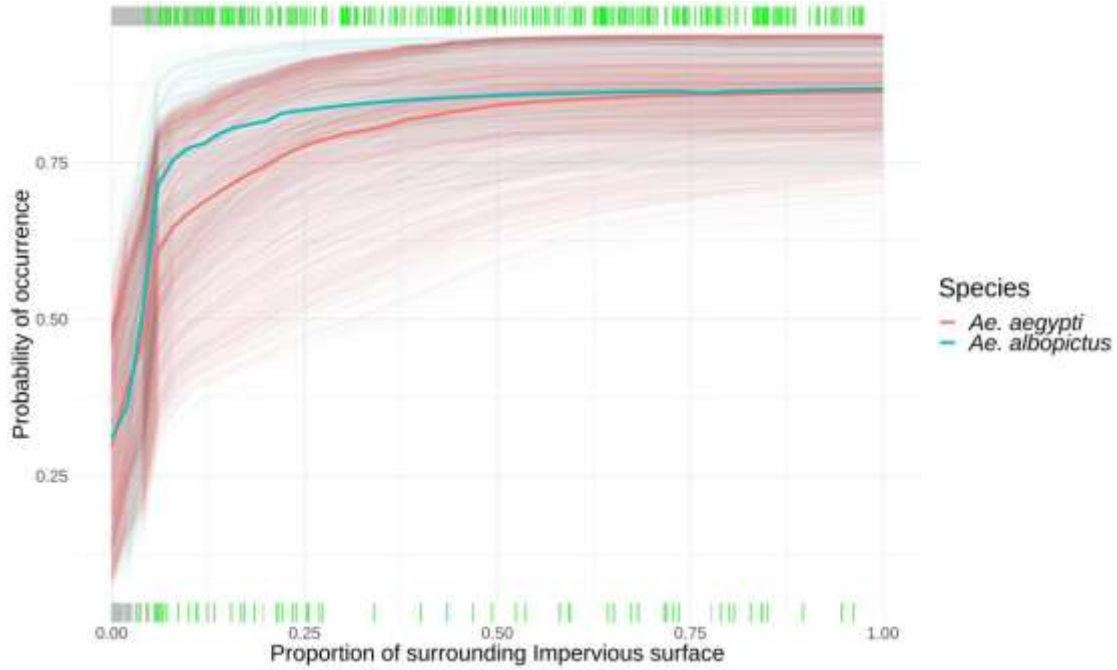

corresponding to occurrences, in grey for values corresponding to pseudo-absences.

Figure S3c. Species Distribution Models partial dependency to all independent variables.

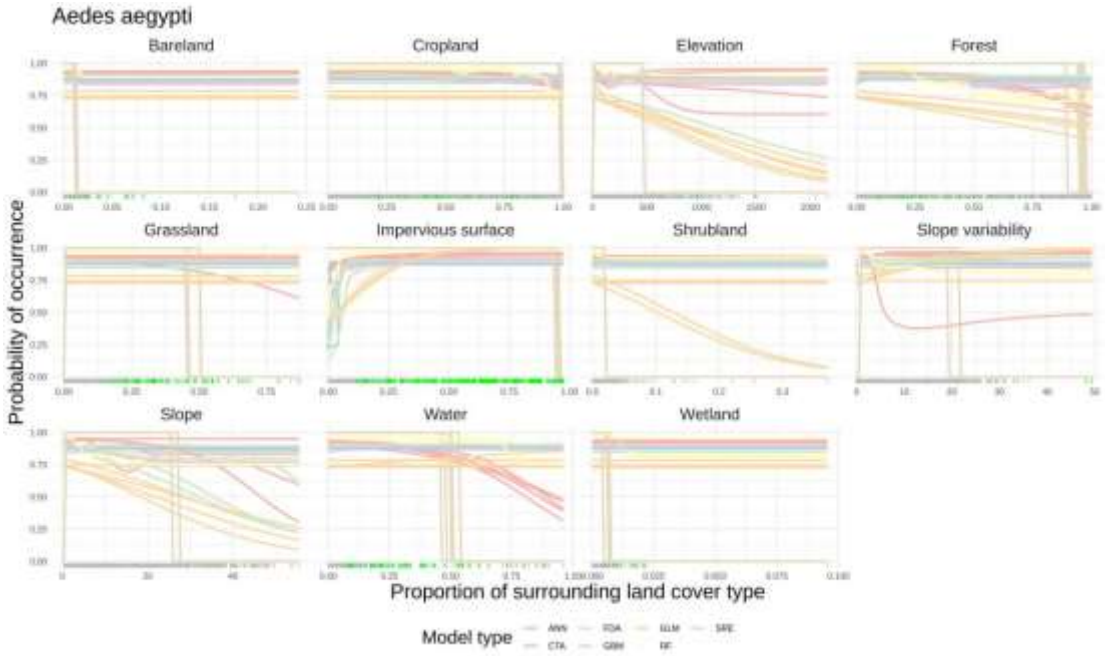

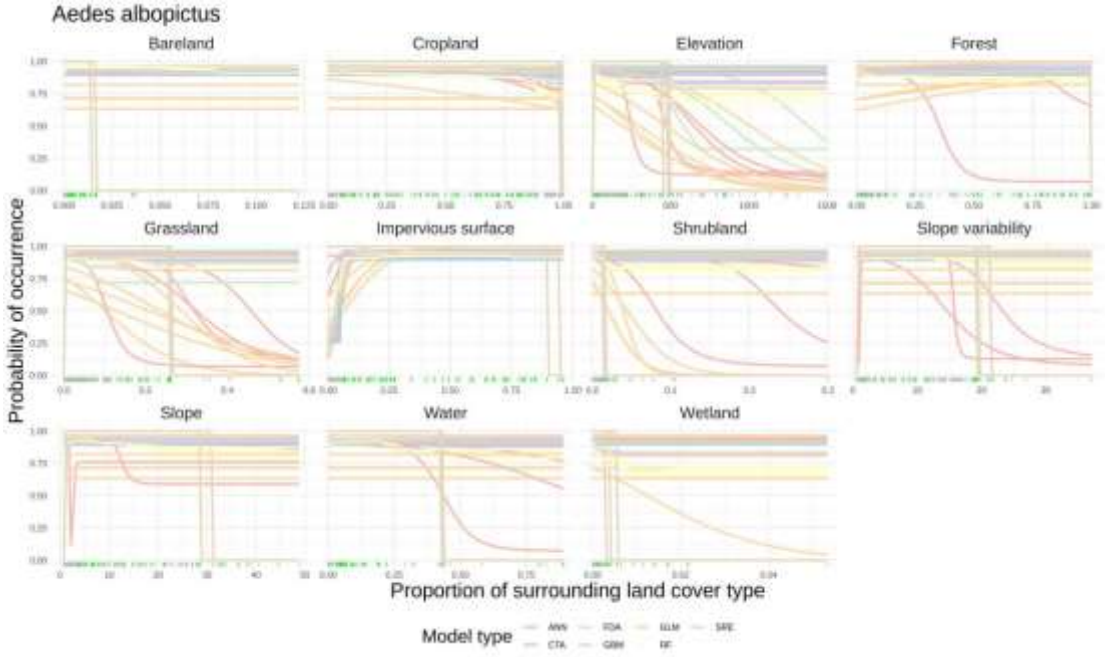

Figure S4. Entomological survey sampling. Sampling locations in Phnom (Cambodia) Penh and Vientiane (Lao PDR) are displayed with red dots.

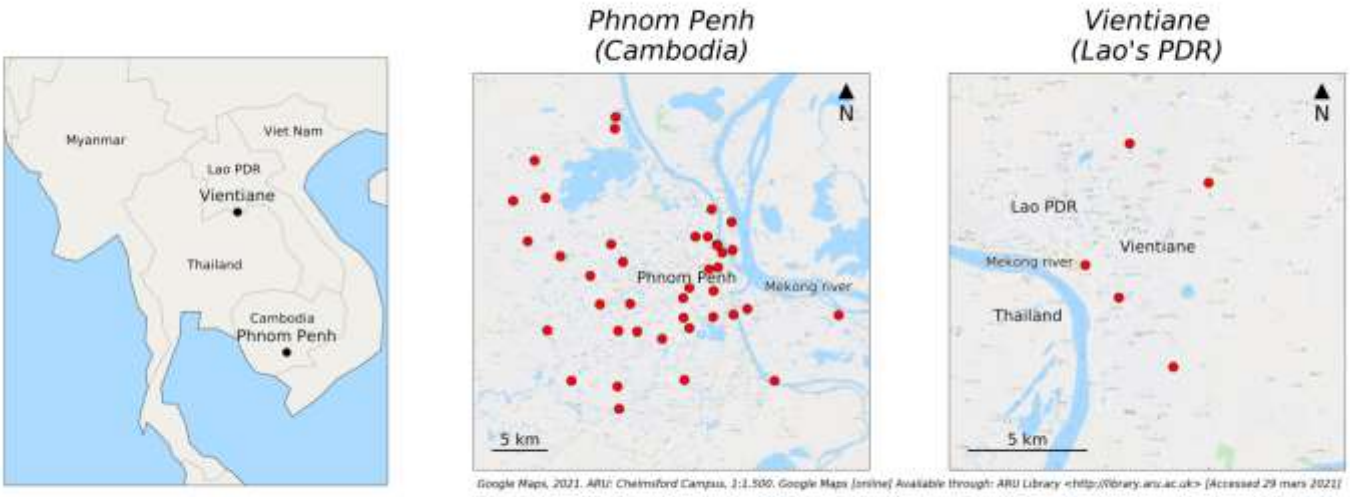

Figure S5. Contemporary climate seasonal variations at sampling sites in Phnom Penh (Cambodia) and Vientiane (Lao PDR).

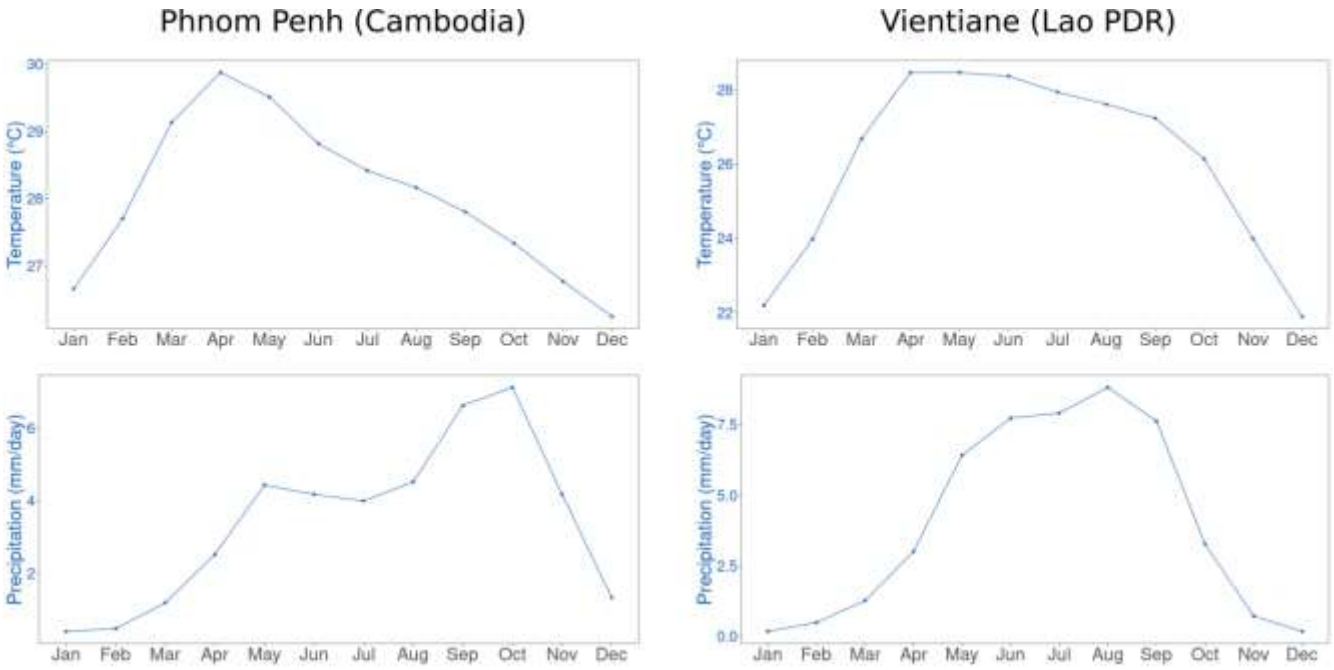

Figure S6. Contemporary temperature and precipitations in Southeast Asia. Spatial and seasonal variations of temperature and precipitation from contemporary data.

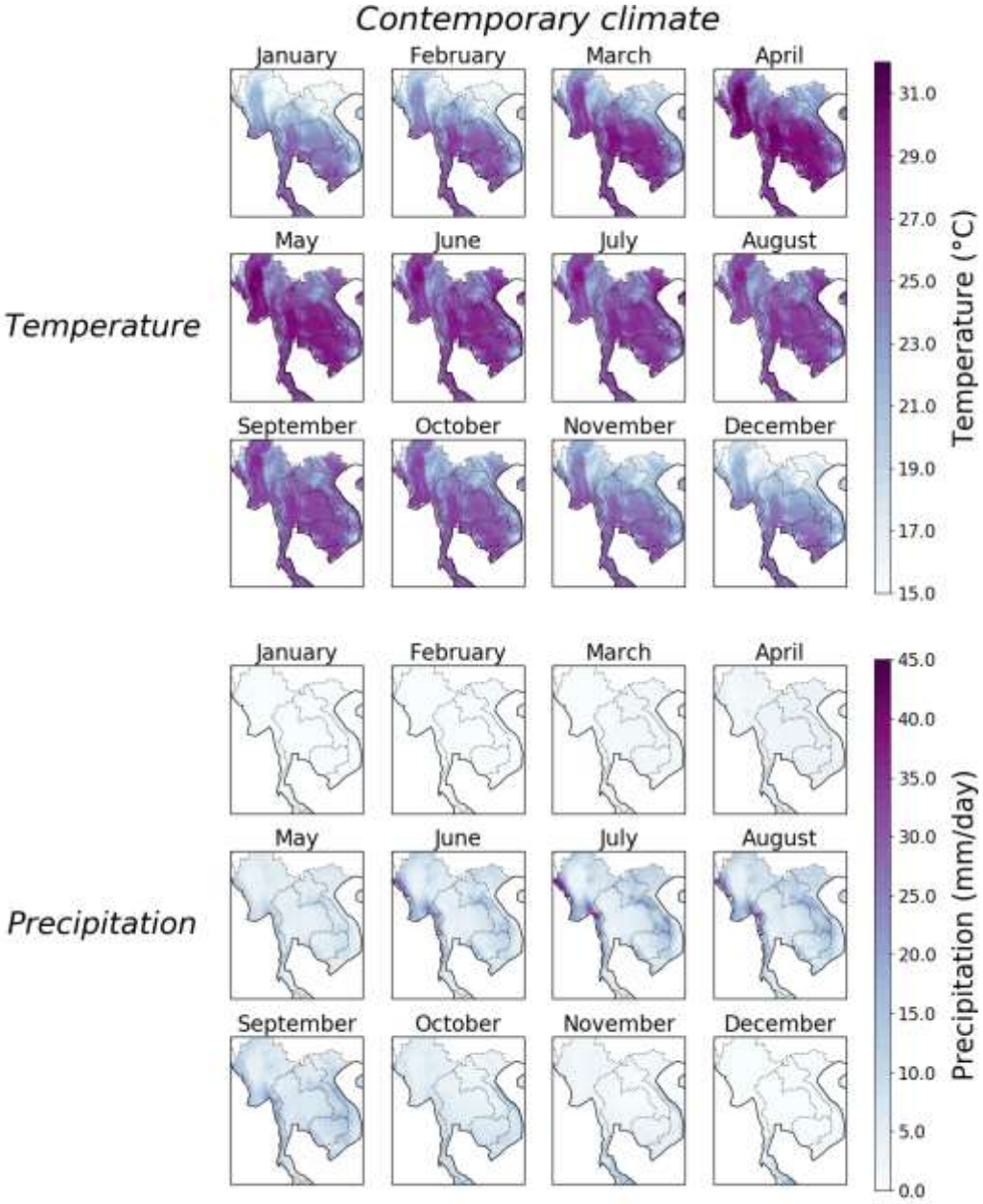

Figure S7. Projected temperature and precipitations in Southeast Asia. Spatial and seasonal variations of climate projections at the end of the century following SSP1 2.3 and SSP3 7.0 (averages of the nine climate models). Diagonal hashing represent grid cells where anomalies associated with the nine climate models are significantly different from 0 (Student's t-test, p-value < 0.05).

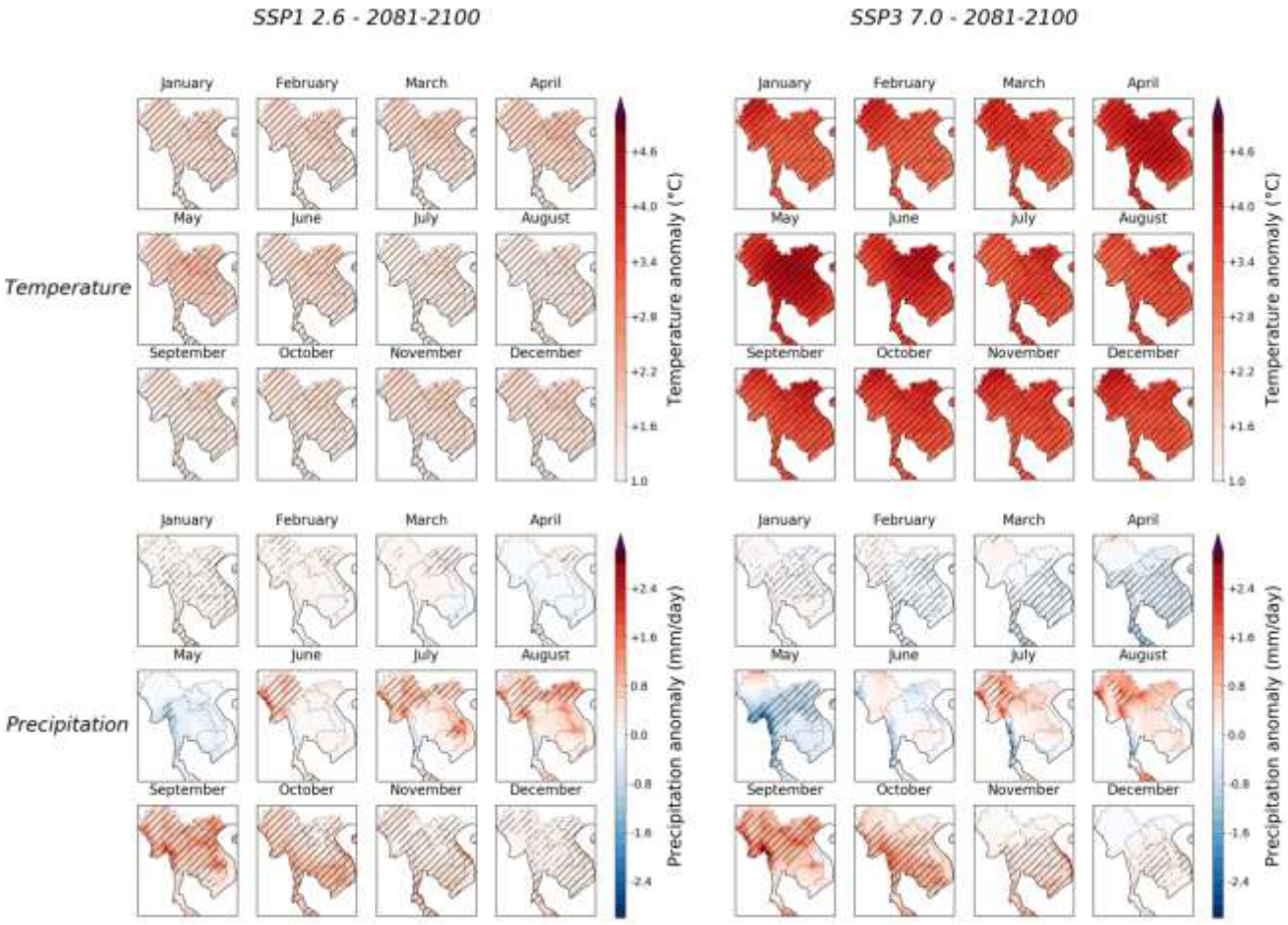

Figure S8. Modeled *Ae. albopictus* and *Ae. aegypti* adult female densities in Southeast Asia, based on contemporary climate. Spatial and seasonal variations of modeled *Aedes* adult female density (top: *Ae. albopictus*; bottom: *Ae. aegypti*), based on contemporary climate data input.

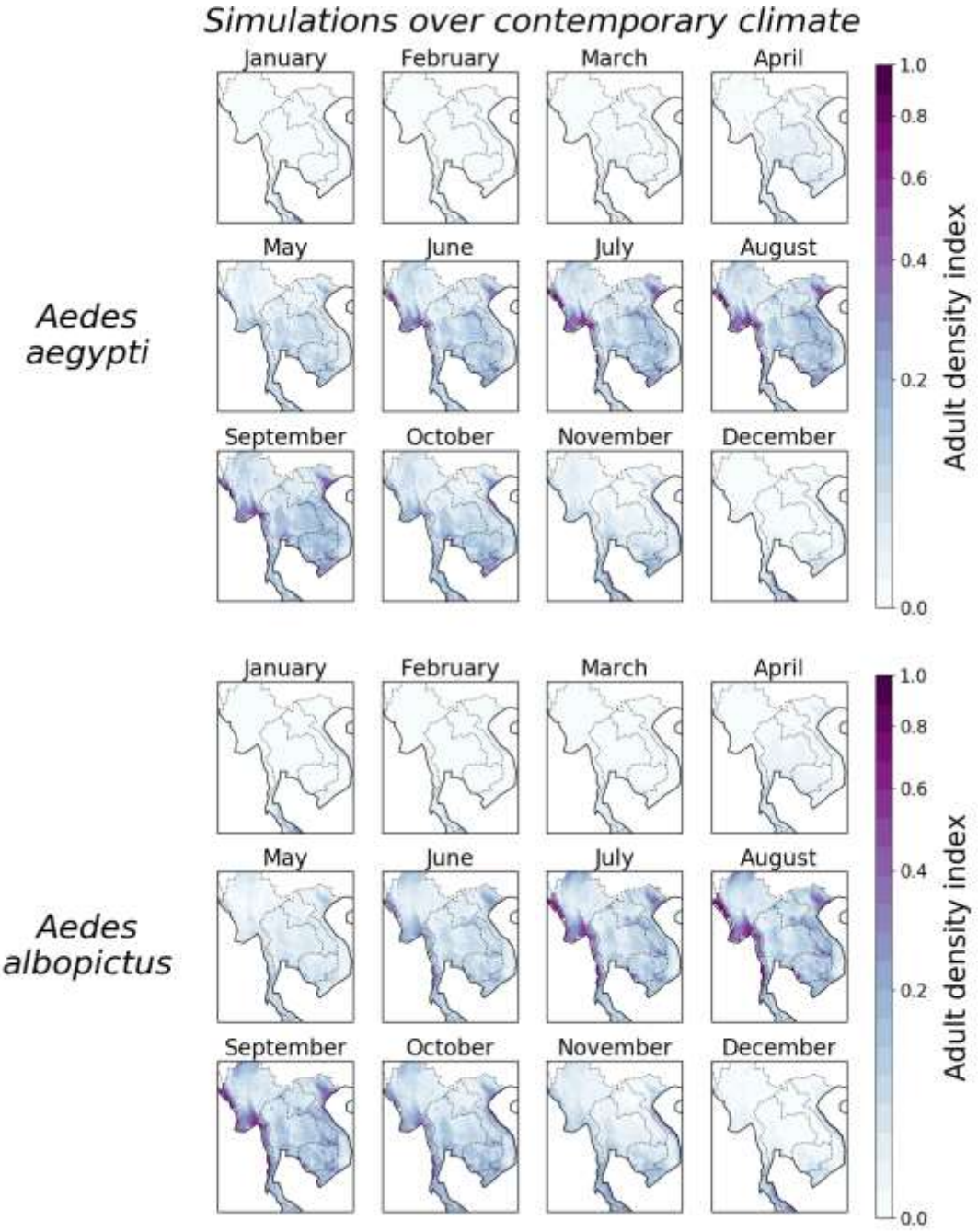

Figure S9. Modeled *Ae. albopictus* and *Ae. aegypti* adult female densities in Southeast Asia, based on future projections. Panels describe projections of modeled *Aedes* adult female density at the end of the century (2081-2100) according to SSP1 2.6 and SSP3 7.0. Percentage changes correspond to ratios of projected modeled density over contemporary modeled densities, averaged over the nine simulations associated with the nine climate models. Positive (red) and negative (blue) percentage changes correspond respectively to higher and lower predicted mosquito density compared to the contemporary situation. Purple grid cells correspond to percentage changes greater than a threshold of 130%, mostly corresponding to areas of null to very low contemporary adult female density. Diagonal hashing represent grid cells where percentage changes associated with the nine climate models are significantly different from 0 (Student's t-test, p-value < 0.05).

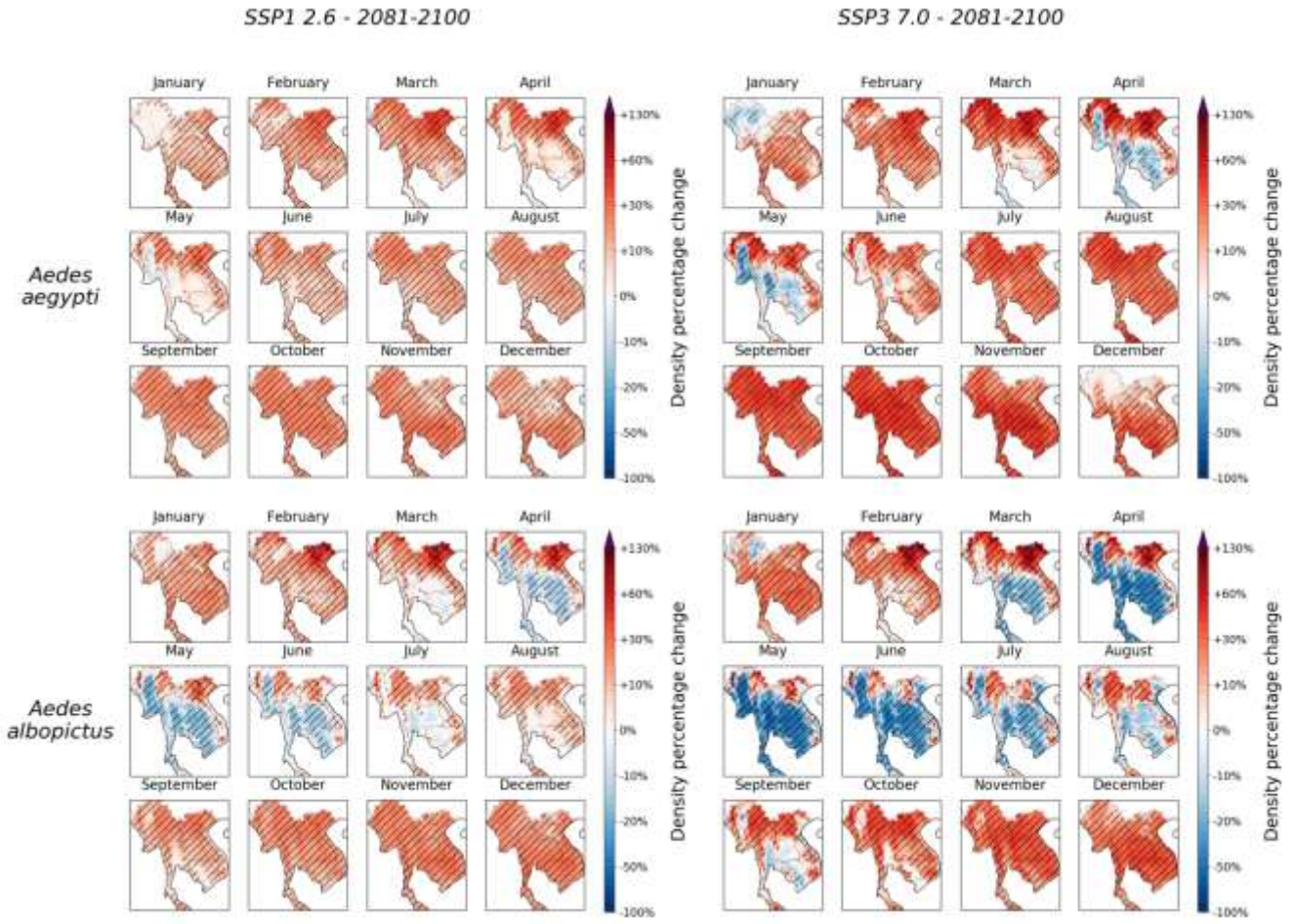

Figure S10. Contemporary climate and future projections during summer and winter months. Panels A describe the spatial variations of contemporary temperature and precipitation in summer (April, May, June) and winter months (December, January, February). Panels B describe projections of temperature and precipitation averaged over the nine climate models in summer and winter months at the middle (2041-2060) and end of the century (2081-2100) according to SSP1 2.6 and SSP3 7.0. Diagonal hashing represent grid cells where anomalies associated with the nine climate models are significantly different from 0 (Student's t-test, p-value < 0.05).

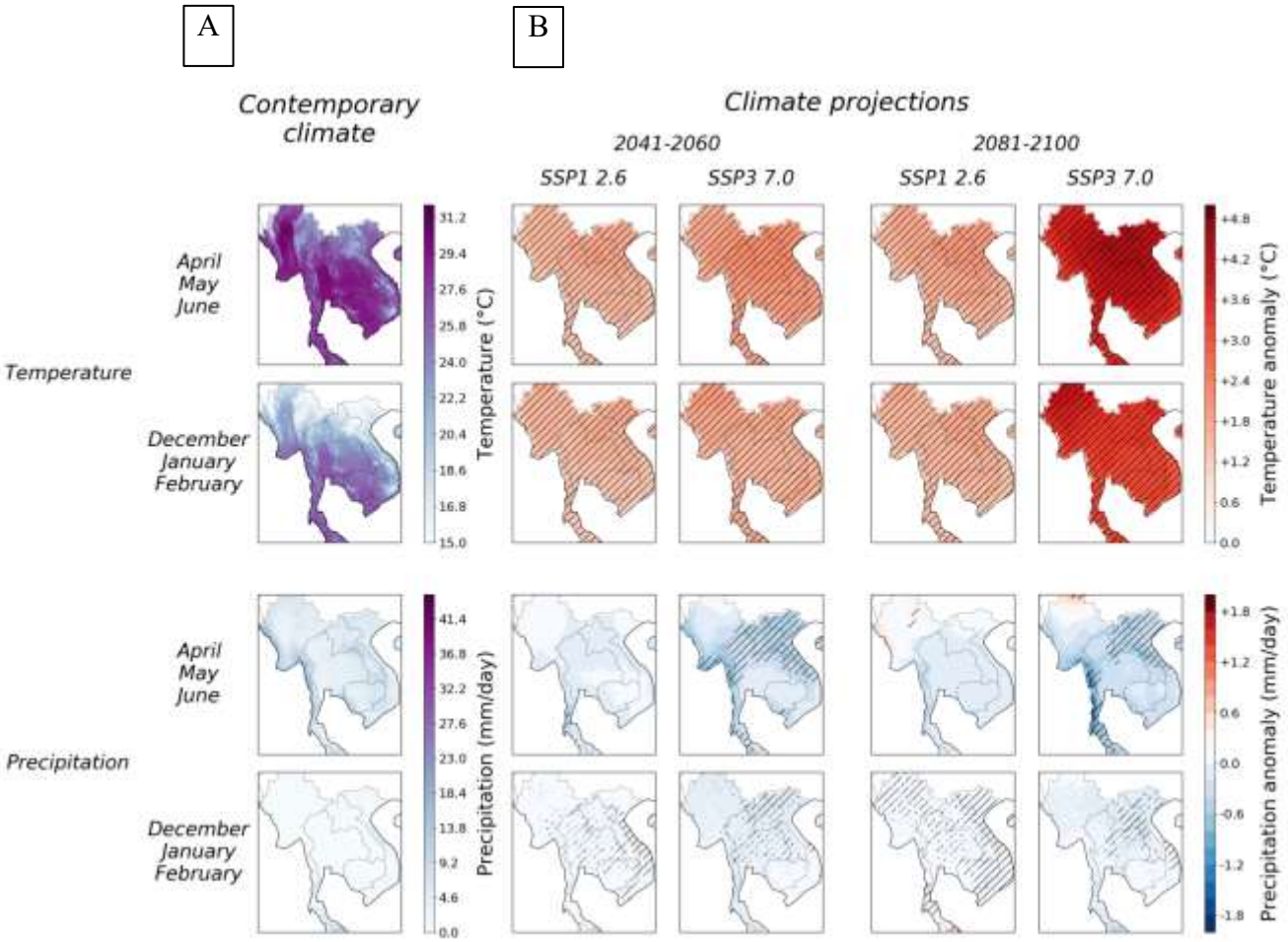

Figure S11. Evolution of modeled *Aedes* density anomalies. Densities of *Ae. albopictus* and *Ae. aegypti* were modeled from climate data averages from all climate models, along the SSP3 7.0 pathway and for four periods to the end of the century. Percentage changes were calculated as a ratio of projected densities over contemporary densities, averaged over the nine simulations associated with the nine climate models. Diagonal hashing represent grid cells where percentage changes associated with the nine climate models are significantly different from 0 (Student's t-test, p-value < 0.05).

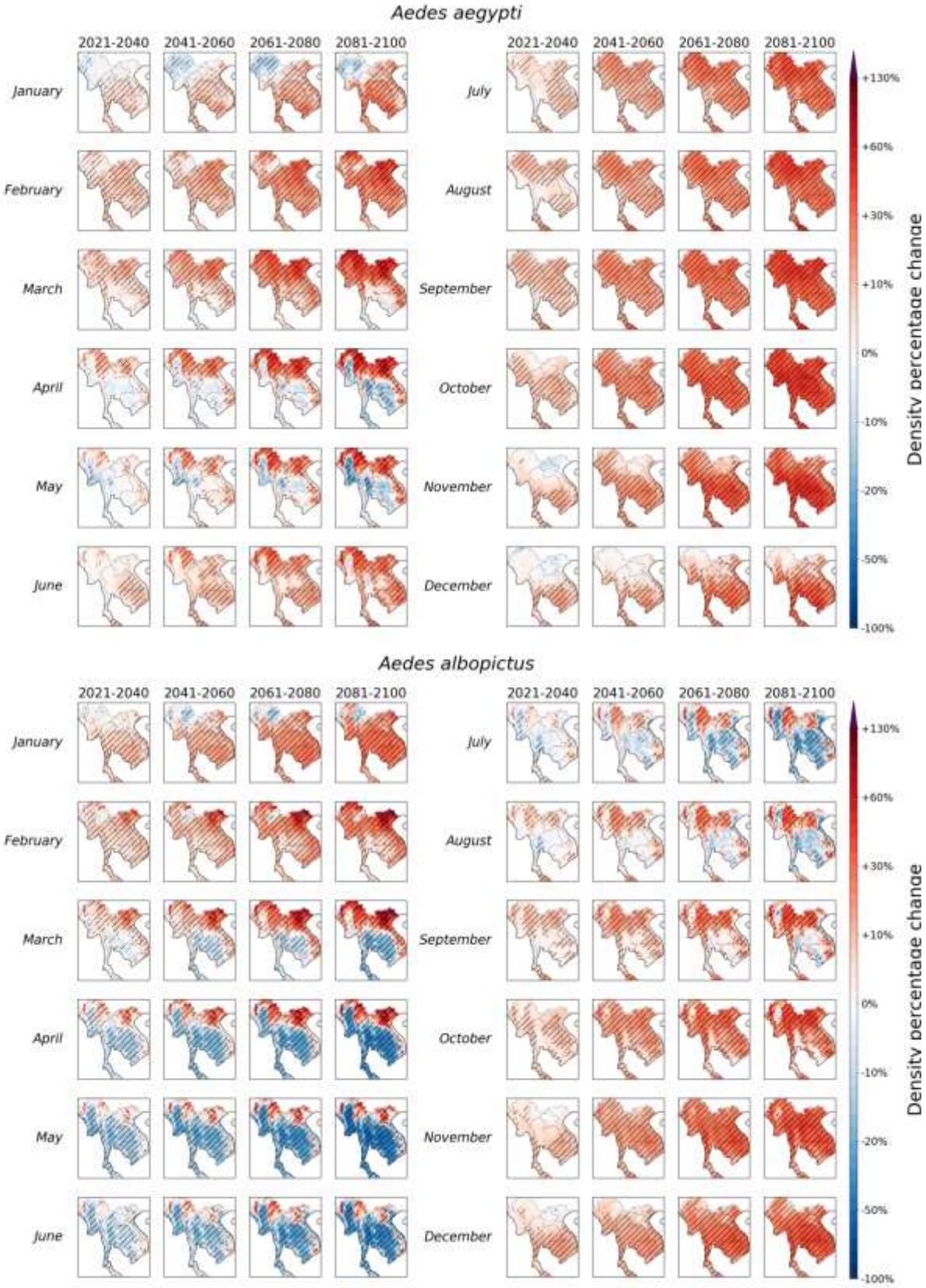
Aedes aegypti
2021-2040
2041-2060
2061-2080
2081-2100
January
February
March
April
May
June
July
August
September
October
November
December
+130%
+60%
+30%
+10%
0%
-10%
-20%
-50%
-100%
Density percentage change
Aedes albopictus
2021-2040
2041-2060
2061-2080
2081-2100
January
February
March
April
May
June
July
August
September
October
November
December
+130%
+60%
+30%
+10%
0%
-10%
-20%
-50%
-100%
Density percentage change

Figure S12. Comparison of modeled *Aedes* density anomalies across Shared Socio Economic Pathways. Densities of *Ae. albopictus* and *Ae. aegypti* were modeled over climate data averages from all climate models, for SSP1 2.6, SSP2 4.5, SSP3 7.0 and SSP5 8.5 and for the 2081-2100 period. Percentage changes were calculated as a ratio of projected densities over contemporary densities, averaged over the nine simulations associated with the nine climate models. Diagonal hashing represent grid cells where percentage changes associated with the nine climate models are significantly different from 0 (Student's t-test, p-value < 0.05).

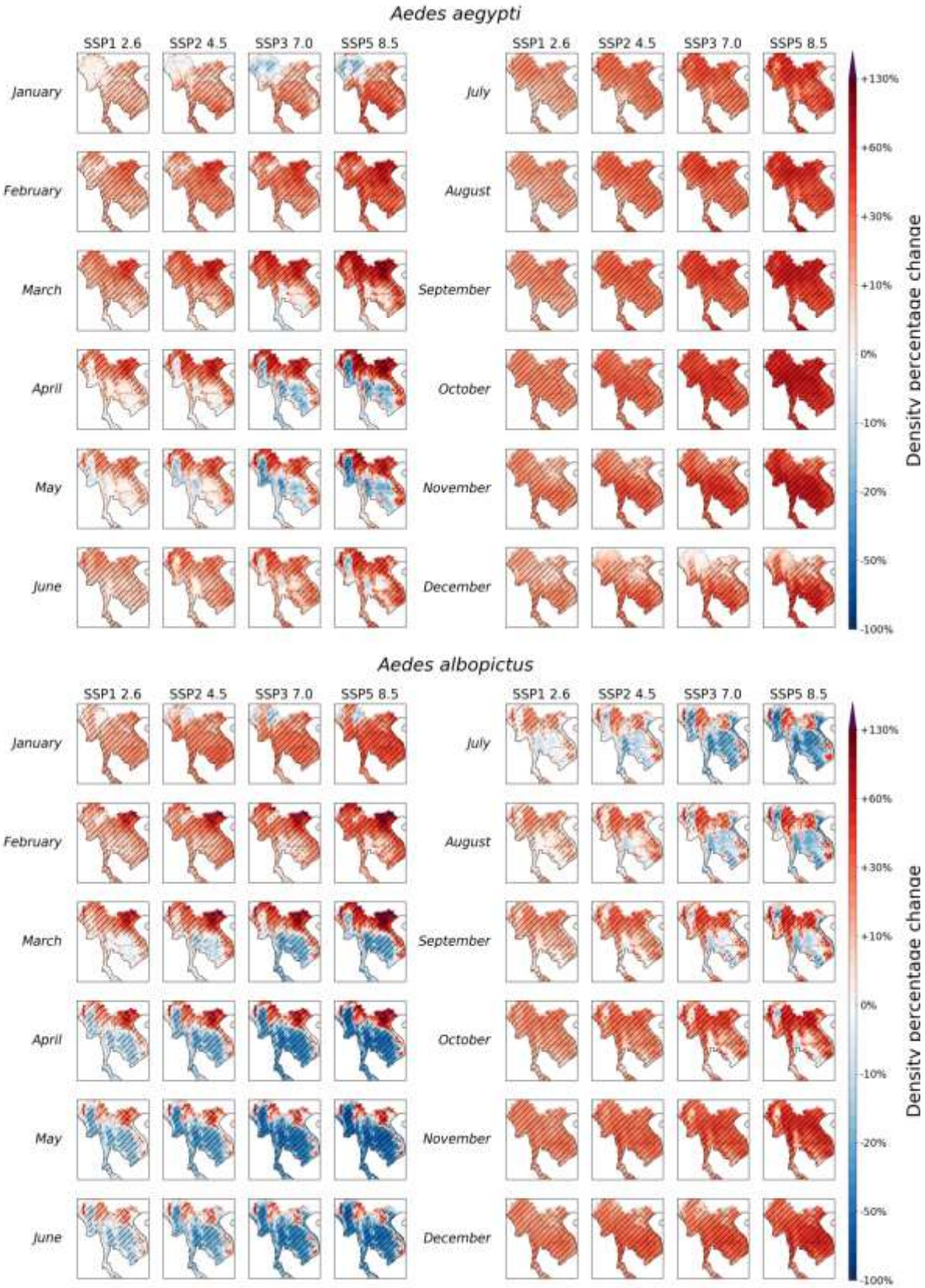
Aedes aegypti
SSP1 2.6
SSP2 4.5
SSP3 7.0
SSP5 8.5
January
February
March
April
May
June
July
August
September
October
November
December
+130%
+60%
+30%
+10%
0%
-10%
-20%
-50%
-100%
Density percentage change
Aedes albopictus
SSP1 2.6
SSP2 4.5
SSP3 7.0
SSP5 8.5
January
February
March
April
May
June
July
August
September
October
November
December
+130%
+60%
+30%
+10%
0%
-10%
-20%
-50%
-100%
Density percentage change

Figure S13. Spatial trends of the future evolution of *Aedes albopictus* density versus topography. Percentage changes correspond to ratios of projected modeled *Ae. albopictus* density in summer months (2081-2100 SSP3 7.0) over contemporary modeled densities, averaged over the nine simulations associated with the nine climate models. Positive (red) and negative (blue) percentage changes correspond respectively to higher and lower predicted mosquito density compared to the contemporary situation. Contour lines represent the 300 m and 600 m isopleths.

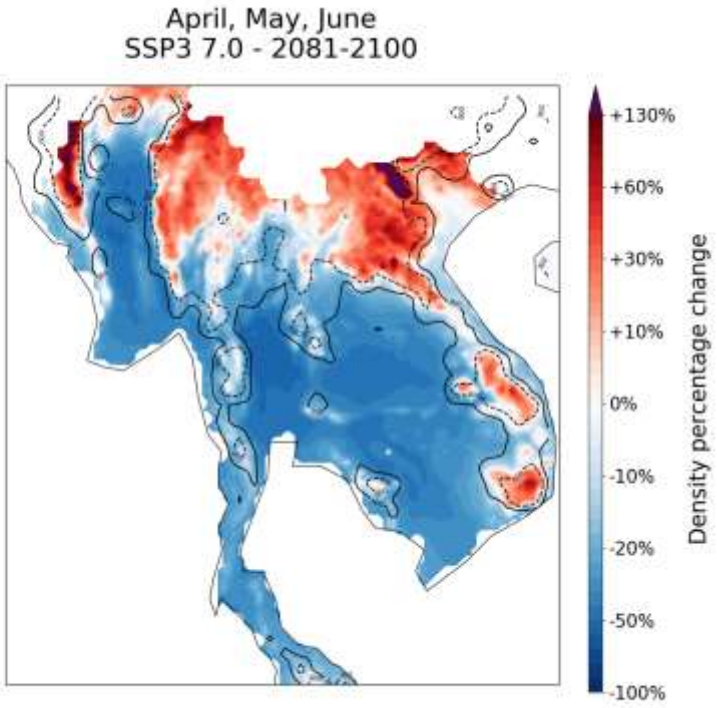

Figure S14. Evolution of projected climate across the 21st century following four Shared Socio-Economic Pathways scenarios. Grid cells were split in two groups considering their elevation (Highlands: elevation < 600 m, Lowlands: elevation > 600 m). For each variable (temperature and precipitation), scenario, period and month, points and bars represent respectively mean and standard deviation of percentage change values associated to all climate models and all grid cells.

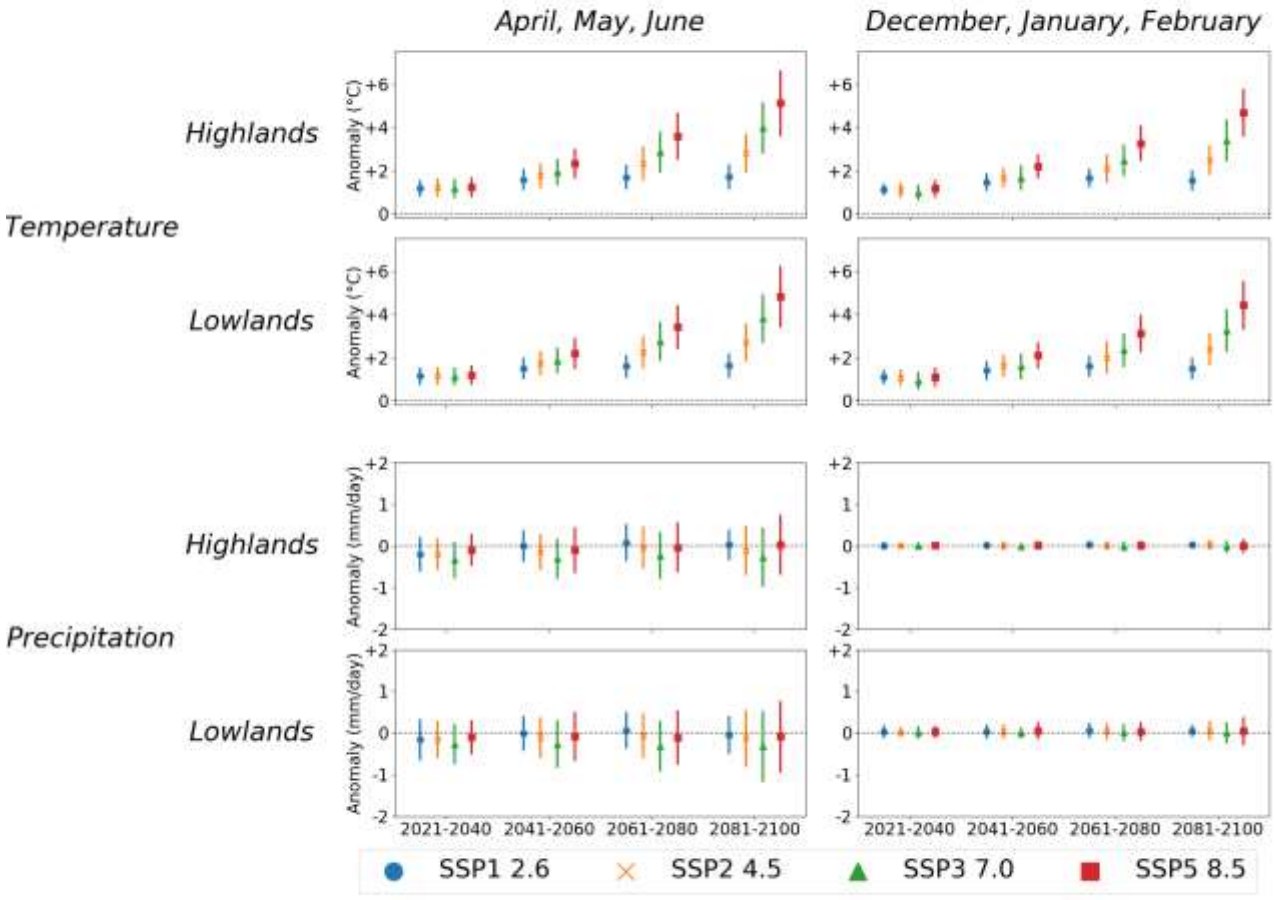

Figure S15. Effects of climate mitigation measures on *Aedes* densities. Process-based model simulations were performed over various constant values of temperature and precipitations. Model outputs were extracted after 30 days of simulation and plotted against corresponding temperature and precipitations (Panels A and C). Changes in temperature and precipitation associated with a transition from SSP3 7.0 to SSP1 2.6 at specific locations and season at the end of the century (2081-2100) are represented with white dots and arrows. Changes in *Ae. aegypti* and *Ae. albopictus* adult densities corresponding to a transition from SSP3 7.0 to SSP1 2.6 at the end of the century are mapped respectively in panels B and D.

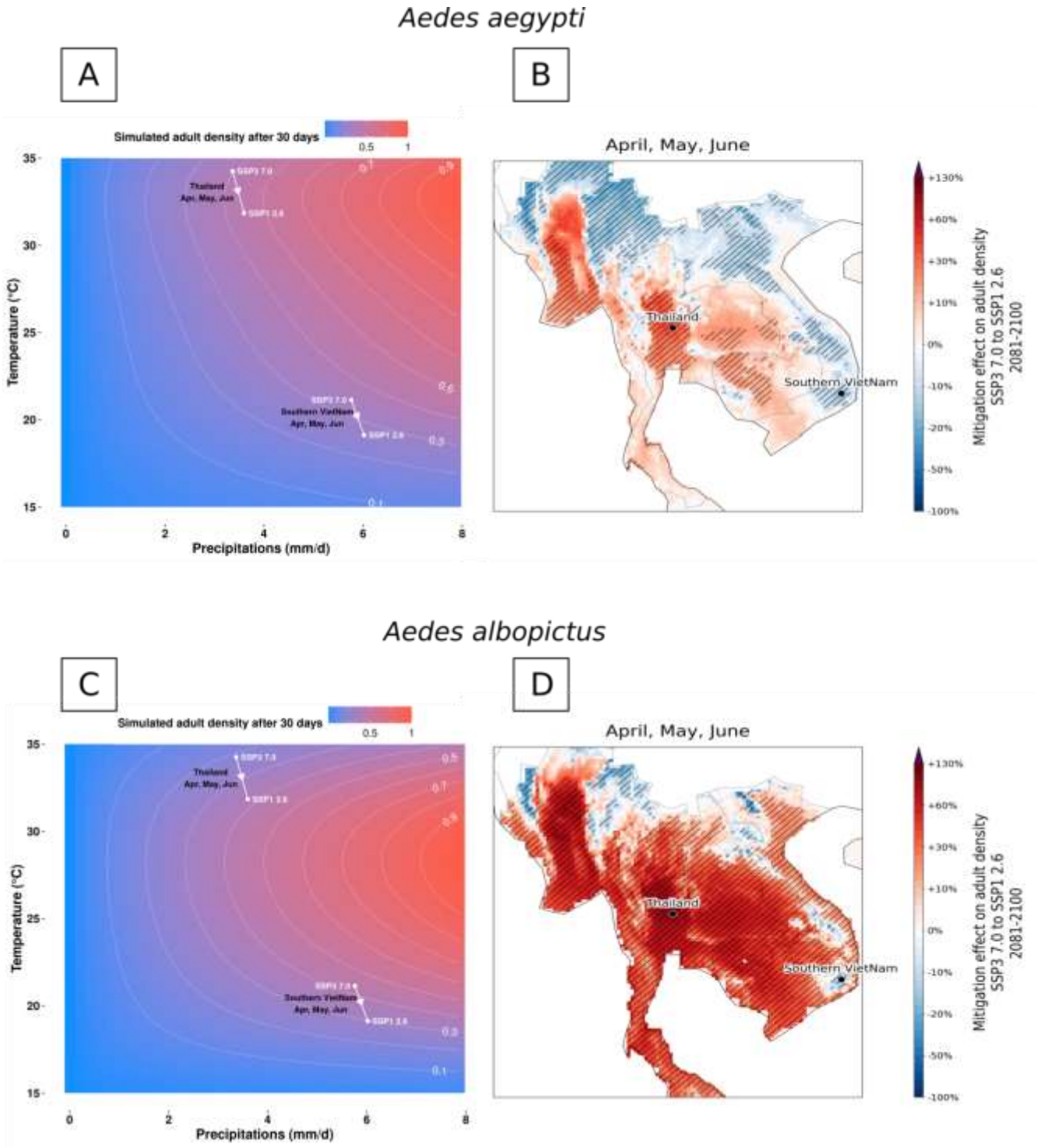

Figure S16. Lengthening/shortening of the *Aedes* high density season. For both species, the median value of daily contemporary density was extracted for each grid cell, thus corresponding to the value at which contemporary densities are greater for 183 days of the year (6 months). For each grid cell, considering a 6-month long season of high contemporary adult density, the length of the season at the 2081-2100 horizon was considered as the number of days projected densities (SSP3 7.0) were greater than the contemporary median value. The lengthening/shortening of the season was assessed as the number of days longer/shorter than the 183 days of the contemporary season. Here are displayed in red and blue the areas where the model respectively predicts a lengthening and a shortening of *Ae. aegypti*'s and *Ae. albopictus*'s season. The values of season lengthening and shortening for each grid cell are displayed for both species as a boxplot (right panel). Boxes extend from quartiles Q1 to Q3, whiskers extend to 1.5 x (Q3 - Q1) from edges of the box. Overall median values are displayed as green bars and correspond to an overall lengthening of 10 days for *Ae. aegypti* and an overall shortening of 4 days for *Ae. albopictus*.

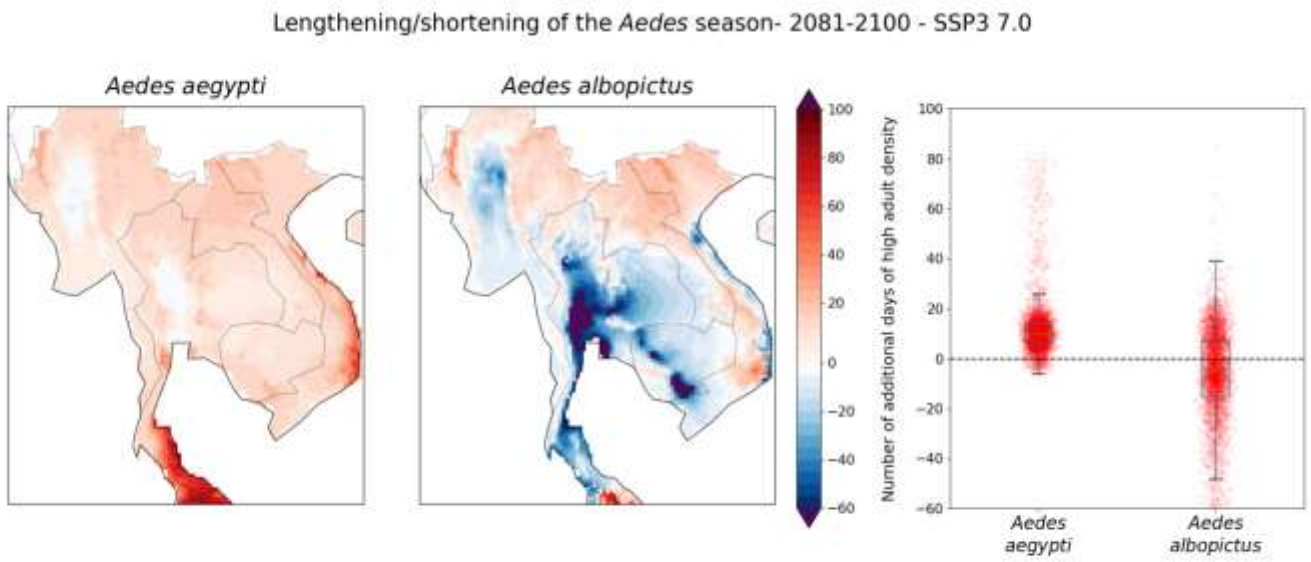

Figure S17. Process-based model's underlying transition and mortality functions as a function of temperature. Panels describe mortality and transition rates between life stages as a function of temperature, as used by the process-based model to simulate population dynamics of *Ae. albopictus* and *Ae. aegypti*.

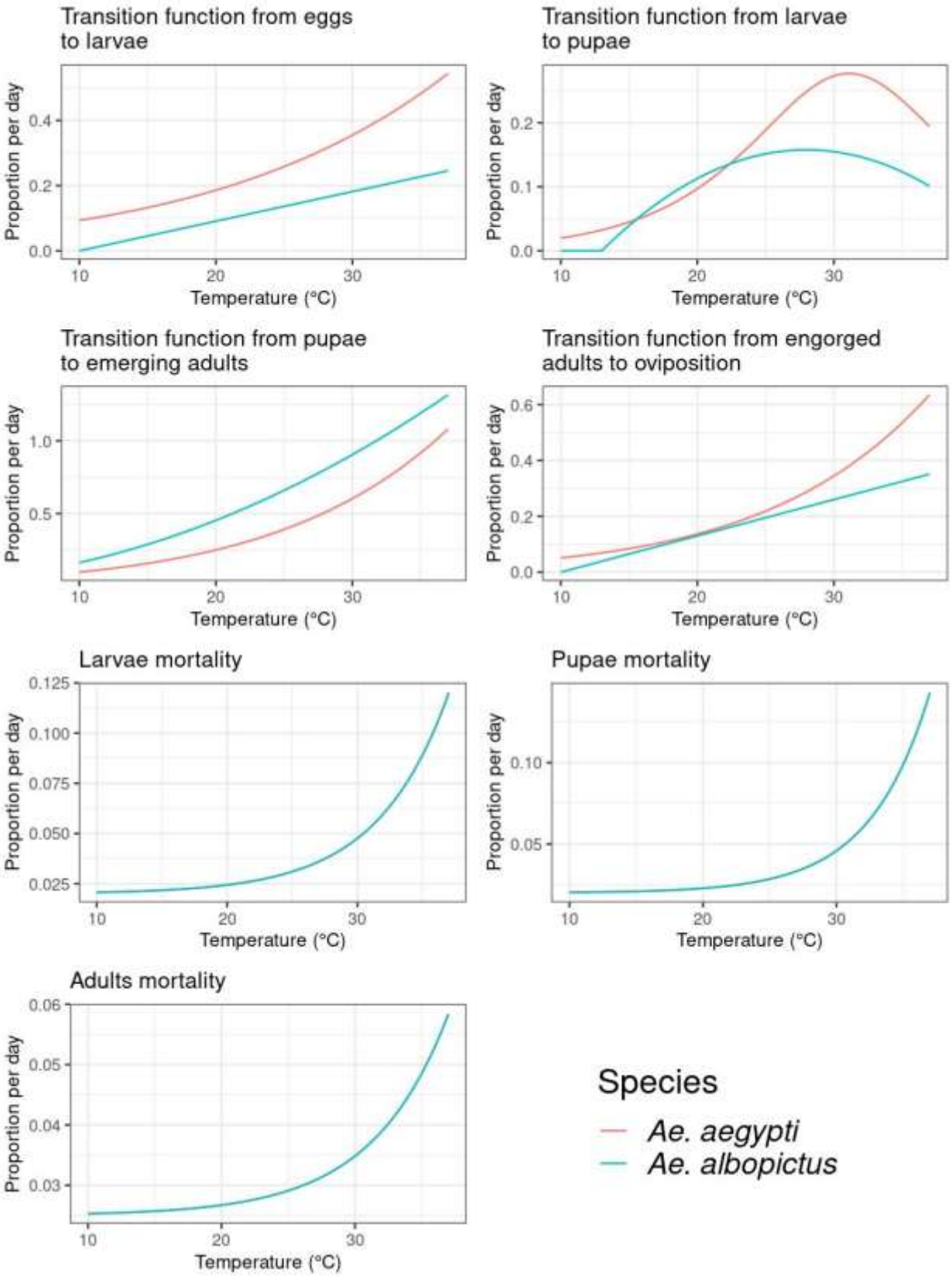
Transition function from eggs to larvae
Proportion per day
0.0
0.2
0.4
10
20
30
Temperature (°C)
Transition function from larvae to pupae
Proportion per day
0.0
0.1
0.2
10
20
30
Temperature (°C)
Transition function from pupae to emerging adults
Proportion per day
0.5
1.0
10
20
30
Temperature (°C)
Transition function from engorged adults to oviposition
Proportion per day
0.0
0.2
0.4
0.6
10
20
30
Temperature (°C)
Larvae mortality
Proportion per day
0.025
0.050
0.075
0.100
0.125
10
20
30
Temperature (°C)
Pupae mortality
Proportion per day
0.05
0.10
10
20
30
Temperature (°C)
Adults mortality
Proportion per day
0.03
0.04
0.05
0.06
10
20
30
Temperature (°C)
Species
Ae. aegypti
Ae. albopictus

Figure S18. Comparison of temperature-dependent transition rates used in process-based models. Temperature-dependent transition rates used in the model developed by Liu-Helmersson et al. (2019),[3] were compared to those used in the present study. Although the two models differed in several aspects, notably on the number of life stages considered, comparing the functions describing transitions rates is still pertinent.

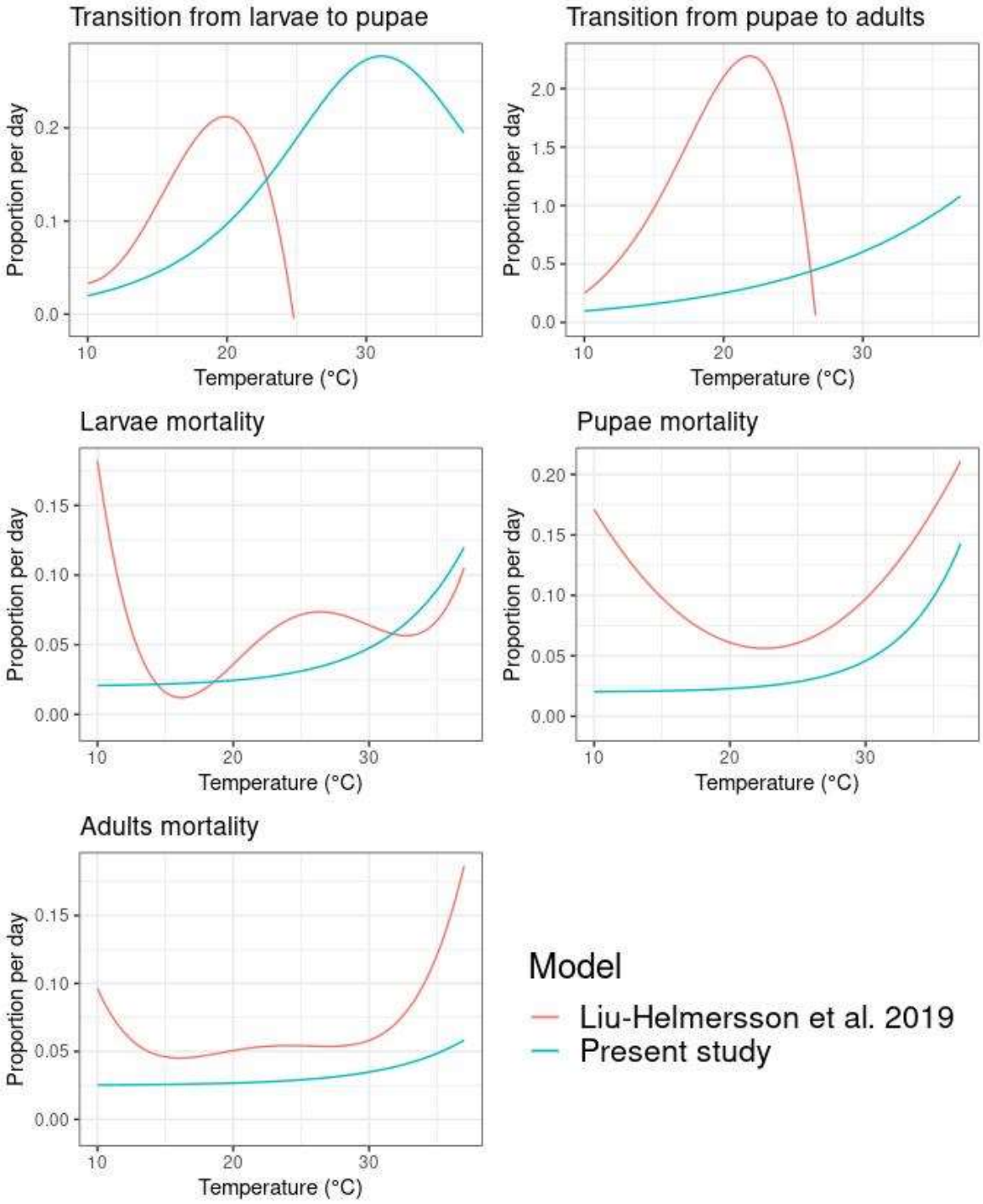

Table S1. Species Distribution Models quality metrics.

Species	Model family	Testing data AUC
Aedes aegypti	GLM	0.88
		0.893
		0.846
		0.86
		0.876
	GBM	0.885
		0.932
		0.886
		0.876
		0.89
	CTA	0.839
		0.864
		0.83
		0.787
		0.803
	ANN	0.88
		0.908
		0.872
		0.865
		0.876
	FDA	0.879
		0.9
		0.863
		0.851
		0.858
	RF	0.884
		0.939
		0.897
		0.883
		0.894
Aedes albopictus	GLM	0.816
		0.694
		0.775
		0.866
		0.882
	GBM	0.938
		0.747
		0.838
		0.896
		0.87
	CTA	0.725
		0.752
		0.755
		0.786
		0.775
	ANN	0.912
		0.608
		0.799
		0.898
		0.895
	FDA	0.84
		0.768
		0.706
		0.831
		0.898
	RF	0.948
		0.769
		0.798
		0.897
		0.875

For each species, the Ensemble modeling process was performed over 6 model families, the 5-fold cross-validation process thus resulted in building 30 models. For *Ae. aegypti*, the 30 models displayed an average AUC of 0.87 (+- 0.03 SD). Ensemble forecasting was performed using the 26 models presenting an AUC>0.85 (colored in black in the following table). For *Ae.*

albopictus, the 30 models displayed an average AUC of 0.84 (+- 0.05 SD). Ensemble forecasting was performed using the 14 models presenting an AUC>0.85 (colored in black in the following table).

Supplemental Material references:

1. Tran, A. *et al.* Complementarity of empirical and process-based approaches to modelling mosquito population dynamics with Aedes albopictus as an example—Application to the development of an operational mapping tool of vector populations. *PLOS ONE* **15**, e0227407 (2020).

2. Kraemer, M. U. G. *et al.* The global compendium of Aedes aegypti and Ae. albopictus occurrence. *Sci. Data* **2**, 1–8 (2015).

3. Liu-Helmersson, J., Brännström, Å., Sewe, M. O., Semenza, J. C. & Rocklöv, J. Estimating Past, Present, and Future Trends in the Global Distribution and Abundance of the Arbovirus Vector Aedes aegypti Under Climate Change Scenarios. *Front. Public Health* **7**, (2019).